TU/e EINDHOVEN UNIVERSITY OF TECHNOLOGY

Experiments and simulations on a cold-flow blast furnace hearth model

Citation for published version (APA):
Nijssen, T. M. J., Hoeks, I., Manjunath, V., Kuipers, H. A. M., van der Stel, J., Adema, A. T., & Buist, K. A. (2022). Experiments and simulations on a cold-flow blast furnace hearth model. *Chemical Engineering Science: X*, *13*, [100120]. https://doi.org/10.1016/j.cesx.2022.100120

Document license:
CC BY

DOI:
10.1016/j.cesx.2022.100120

Document status and date:
Published: 01/02/2022

Document Version:
Publisher's PDF, also known as Version of Record (includes final page, issue and volume numbers)

Please check the document version of this publication:

• A submitted manuscript is the version of the article upon submission and before peer-review. There can be important differences between the submitted version and the official published version of record. People interested in the research are advised to contact the author for the final version of the publication, or visit the DOI to the publisher's website.
• The final author version and the galley proof are versions of the publication after peer review.
• The final published version features the final layout of the paper including the volume, issue and page numbers.

Link to publication

General rights
Copyright and moral rights for the publications made accessible in the public portal are retained by the authors and/or other copyright owners and it is a condition of accessing publications that users recognise and abide by the legal requirements associated with these rights.

• Users may download and print one copy of any publication from the public portal for the purpose of private study or research.
• You may not further distribute the material or use it for any profit-making activity or commercial gain
• You may freely distribute the URL identifying the publication in the public portal.

If the publication is distributed under the terms of Article 25fa of the Dutch Copyright Act, indicated by the "Taverne" license above, please follow below link for the End User Agreement:

www.tue.nl/taverne

Take down policy
If you believe that this document breaches copyright please contact us at:

openaccess@tue.nl

providing details and we will investigate your claim.

Download date: 24. Feb. 2023

Chemical Engineering Science: X 13 (2022) 100120

Contents lists available at ScienceDirect

Chemical Engineering Science: X

journal homepage: www.elsevier.com/locate/cesx

Experiments and simulations on a cold-flow blast furnace hearth model

Tim M.J. Nijssen [a], Indy Hoeks [a], Vishwanath Manjunath [a], Hans A.M. Kuipers [a], Jan van der Stel [b], Allert T. Adema [b], Kay A. Buist [a,*]

[a] Multiphase Reactors Group, Department of Chemical Engineering & Chemistry, Eindhoven University of Technology, P.O. Box 513, 5600 MB Eindhoven, the Netherlands
[b] Research and Development, Tata Steel Europe, P.O. Box 10.000, 1970 CA IJmuiden, the Netherlands

ARTICLE INFO

Article history:
Received 7 October 2021
Received in revised form 10 November 2021
Accepted 21 January 2022

Keywords:
Ironmaking
Blast furnace
Deadman
CFD-DEM
Magnetic Particle Tracking

ABSTRACT

The blast furnace hearth plays an important role in the operational stability and lifetime of the reactor. The quasi-stagnant bed of coke particles termed the deadman undergoes complex interaction with the flowing hot metal, and remains largely ill-understood. In this work, a cold model blast furnace hearth is presented, and studied using both numerical and experimental techniques. Magnetic Particle Tracking (MPT) is used to investigate the individual particle behaviour within the cylindrical, opaque bed. At high liquid holdup, the particle bed was found to alternate between floating and sitting states, following the liquid level during the tapping and filling cycle. This bed motion was found to induce a migration of particles, thereby slowly renewing the deadman. The rate of horizontal migration increases with the vertical bed amplitude, and the renewal of particles is concentrated around the opening of the tap hole. No direct influence of the coke-free space on the tapping rate was found in these experiments. Instead, the disturbance of the packing in front of the tap hole was observed to lead to a higher tapping rate. Additionally, a coupled numerical framework is presented, in which Computational Fluid Dynamics (CFD), the Volume of Fluid (VOF) method and the Discrete Element Method (DEM) are combined. A simulation set-up is presented which closely replicates the experimental conditions. The position and movement of the floating bed are found to be well-predicted by the VOF/CFD-DEM model. Particle trajectories are presented, and migration of particles within the deadman is observed. Alongside the particle motion, the liquid flow pattern during draining of the vessel is visualised. It is concluded that a coke-free space underneath the deadman significantly impacts the shape of the liquid flow pattern, which affects the erosion processes within the blast furnace hearth.

© 2022 The Author(s). Published by Elsevier Ltd. This is an open access article under the CC BY license (http://creativecommons.org/licenses/by/4.0/).

1. Introduction

It has been widely accepted that an improved understanding of the phenomena in the lower zone of the blast furnace is of paramount importance to obtain more stable furnace operation and extended campaign lifetimes (Andreev et al., 2017; Dong et al., 2007). Among the extensive research conducted to gain insight into this large and complex reactor, an attractive alternative approach is the use of lab-scale cold-flow models. Due to the practical limitations and difficulties involved with experiments using hot liquid metal, many researchers have resorted to cold-flow experiments. In such work, the hot blast gas, ore and coke particles, and liquid iron and slag are replaced by model substances, often using room-temperature air, water and oil as gas, iron and slag respectively. This approach greatly widens the range of available experimental techniques and allows for a safer and more accessible study of blast furnace phenomena, provided that materials and conditions are selected appropriately.

1.1. Cold model blast furnace research

Over the past years, all aspects and sections of the blast furnace have been extensively investigated using such cold-flow experiments. For example, Jimenez et al. (2000) investigated the charging of the ore and coke burden in a scaled half-section blast furnace model, and revealed the influence of the upward gas flow on the final burden distribution and layer structure. The descent of the burden through the blast furnace shaft was studied by Takahashi et al. (1996), providing valuable insights into the solids flow patterns within the upper furnace and visualising the formation of the deadman zone. Other extensively investigated aspects of the blast furnace are the coke-free raceways and the solids flow around them, which were studied using cold flow experiments by Takahashi and Komatsu (1993).

* Corresponding author.
E-mail address: K.A.Buist@tue.nl (K.A. Buist).

https://doi.org/10.1016/j.cesx.2022.100120
2590-1400/© 2022 The Author(s). Published by Elsevier Ltd.
This is an open access article under the CC BY license (http://creativecommons.org/licenses/by/4.0/).

The lower section or hearth of the blast furnace has recently been gaining increasing attention from researchers, as its internal phenomena are widely believed to be decisive for the furnace campaign lifetime (Andreev et al., 2017). Experimental studies on this subject matter commonly focus on either the flow of the immiscible iron and slag phases during tapping, or the behaviour of coke particles in the deadman zone. One of the earliest cold-flow studies of the multi-phase tapping was conducted by Tanzil et al. (1984), by use of water glycerol mixtures and mercury to represent the slag and iron phases, respectively. Their work revealed the well-known tilting of the slag interface towards the taphole and provided insight into the residual volumes of slag and iron remaining in the furnace after tapping. More recently, the experiments of Nouchi et al. (2003) showed how the coke bed structure directly in front of the taphole strongly influences the attainable tapping rates. He et al. (2012) investigated the effects of coke-free space under the deadman on the tapping behaviour, and found that the coke-free space allows for longer tapping times and lower residual liquid volumes.

Aside from the liquid flow in the hearth, the movement of coke particles in the lower section of the blast furnace has been studied as well. The solid flow of a floating particle bed subject to discharge was studied by Nouchi et al. (2003,), who employed a model system consisting of a bed of wooden spheres floating in water. They found the liquid level (i.e. the balance between gravity and buoyancy) to be of great importance to the solid flow patterns. The deadman renewal inside a 2D model blast furnace was investigated experimentally by Shibata et al. (1990), using room-temperature air, water and low-density particles. They found that in between tapping cycles, the deadman particles rise towards the raceways, forming a coke-free space underneath the bed. The shape of this coke-free space was found to significantly affect liquid flow patterns and the heat-load on the furnace walls. A similar study was conducted by Takahashi and Kawai (2001), using a half-section model blast furnace. Their work specifically focused on particle movement patterns within the deadman, and revealed two renewal mechanisms: particles close to the deadman surface can get pushed into the active flowing layer by the rising liquid level, whereas particles deeper in the bed slowly migrate towards to raceways in a zig-zag fashion. The authors concluded that the rising and falling liquid level within the hearth and the resulting floating and sinking of the particle bed were the driving force behind the deadman renewal. Later, they were able to reproduce these findings using DEM simulations (Kawai and Takahashi, 2004). Nogami et al. (2004) were able to further investigate the mechanisms of deadman renewal, and quantified the residence time of coke particles based on their location within the deadman. A more shallow hearth geometry and a larger accumulated volume of liquid were found to decrease the residence time i.e. accelerate deadman coke renewal.

1.2. Blast furnace modelling

Aside from experimental methods, mathematical and numerical modelling are highly prominent tools applied in blast furnace research. Such approaches offer many distinct advantages over laboratory or *in situ* experiments, such as being safer, less expensive, and offering an improved insight in the otherwise inaccessible system.

Early blast furnace models used 1D, steady-state mathematical models built upon mass and energy conservation equations. Later, these models have been extended to represent the transient process of the full 3D blast furnace (Ariyama et al., 2014). A notable example of such a method is the four-fluid model introduced by Yagi (1993), Austin et al. (1997). In their work, the furnace is represented by four continuous phases: gas, liquid, solid and powder. By considering the motion of these phases and the mutual interactions between them, the mechanical, thermal and chemical processes in the reactor could be represented.

While continuum models, such as the four-fluid model, provide useful results for large-scale furnaces, their representation of the solid phase is inherently limited, especially for zones where multiple and enduring particle contacts prevail. In order to describe the discrete particle phase as a continuous medium, constitutive relations describing the solid flow behaviour are used. In doing so, essential information on the particle-scale is lost, and the macroscopic influence of microscopic properties and phenomena cannot be captured. Fortunately, the continual development of high-performance computers has enabled more sophisticated computational methods, in which particles can be treated as discrete entities.

In the Discrete Element Method (DEM) pioneered by Cundall and Strack (1979), particles are considered individual entities whose movement is described by Newtons laws of motion. Both Nouchi et al. (2003,) and Kawai and Takahashi (2004) conducted experiments on the solid flow behaviour of the burden descending in the blast furnace, and were able to reproduce their results using DEM. Nouchi et al. (2005) expanded their simulation to a full-scale blast furnace, and visualised the solids flow patterns and stress distribution within the reactor. In order to minimise the computational cost of their simulations, a small pie-slice geometry was used instead of a full 3D reactor. Zhou et al. (2005) determined that such a pseudo-2D approach overestimates the deadman size due to increased particle-particle and particle-wall interactions, and a 3D approach must be adopted to accurately simulate the blast furnace. Ueda, Fan, Natsui, and Zhang et al. conducted various studies, investigating the influence of particle properties (Ueda et al., 2010), working volume (Fan et al., 2010), asymmetrical combustion zones (Natsui et al., 2010), and shaft and bosh angles (Zhang et al., 2011) on the macroscopic solid-flow patterns. These studies exemplify the investigation of microscopic phenomena and their macroscopic effects, which cannot be attained using continuum methods.

Aside from discrete methods, continuum-based methods have also been extended as a result of improved computational infrastructure. Modern Computational Fluid Dynamics (CFD) have been applied to the blast furnace, especially to study the flow of liquid iron and slag during tapping. Takatani et al. (2001) studied the tapping process and resulting erosion with different pre-determined deadman shapes, and found that the coke-free space and low permeability of the bed promote wall erosion. Similarly, Panjkovic et al. (2002) studied the flow and heat transfer in different industrial hearth geometries, and compared the obtained temperature distributions with plant data. They obtained a good correspondence of their model in case of a sitting deadman, but found discrepancies near the hearth bottom in case of a floating deadman, possible due to an ill-defined shape of the coke-free layer. Shao and Saxén (2013), Shao (2013) studied the two-phase flow of iron and slag in the blast furnace hearth and taphole, and found that both Volume of Fluid (VOF) and Two Fluid Model (TFM) formulations can be employed to accurately describe the system.

In recent years, the combination of continuum-based and discrete approaches into the CFD-DEM method has gained popularity for blast furnace research. In this approach, the solid phase is treated as discrete particles, while the flow of the continuous phases (gas and/or liquid) through this particle bed is evaluated using CFD methods. Feng et al. (2003) used this approach to simulate the formation of the coke-free raceway zones. Later, the same research group (Zhou et al., 2010) was able to integrate this into a complete CFD-DEM model of a small-scale, 2D blast furnace. In this work, only the gas flow was considered, while the liquid was modelled as a dynamic zone of increased buoyancy. The results

of this study have shown how the internal state of the blast furnace is an intricate interplay between gravity, buoyancy and pressure drop, which can be accurately captured by the CFD-DEM method. A similar study was conducted by Adema et al. (2010), Adema (2014), who included the effects of non-spherical particle shape and compared different types of simulation domains.

Vångö et al. (2018, 2019) integrated the CFD-DEM method with the Volume of Fluid (VOF) methodology, which allowed them to include multiple continuous phases and simulate the iron-slag and slag-gas interfaces in the blast furnace hearth. Combined with a database-driven model for the deadman position and porosity, they were able to perform long-term simulations of a full-scale blast furnace hearth. By comparing simulations using static and dynamic deadman models, they concluded that the bed movement during tapping significantly influences the liquid flow, and the deadman cannot be accurately modelled in a static fashion. A similar VOF/CFD-DEM approach was employed by Bambauer et al. (2018), who simulated the solid, gas and liquid flow in a complete small-scale blast furnace. They observed the effects of liquid level on the deadman shape, and found circulation of particles inside the deadman down the reactor centre and up along the hearth walls.

1.3. Current work

Virtually all authors mentioned in Section 1.1 employed optical methods for investigation of particle movement within the experimental setup. Optical methods are accessible and readily available, especially when the system under investigation is slow enough to exclude the necessity of high-speed cameras. However, these optical methods rely on continuous visibility of the tracer particle(s), thereby limiting all research to 2D or pseudo-2D systems. For blast furnace research, this means that either 2D slot geometries (e.g. Shibata et al. (1990)) or half-section geometries (e.g. Takahashi and Kawai (2001)) must be used. The inevitable wall-effects introduced by these geometries can significantly influence particle behaviour and alter solid flow patterns, as was shown by (Bambauer et al., 2018).

In this work, Magnetic Particle Tracking (MPT) is used to study the deadman particle behaviour in a cold model blast furnace hearth. The MPT technique, in which a single magnetic tracer particle is tracked over time by an array of magnetic field sensors, allows for the study of particle behaviour within a full 3D model set-up, as it does not rely on optical visibility of the tracer. A model hearth set-up is presented, in which the deadman behaviour is separated from the rest of the blast furnace. By use of extensive automation of the set-up, a variety of operational and geometric conditions can be created, and long-term experiments can be conducted. Using this new set-up, particle movement within the blast furnace hearth is studied, and the influences of the sump depth (i.e. the distance from tap hole to the hearth bottom) and the tapping cycle length are investigated.

In addition to the experimental work, the VOF/CFD-DEM method developed by Vångö et al. (2018) is combined with a liquid-solid momentum coupling (Nijssen et al., 2020). This combined method is then used to simulate the 3D model blast furnace hearth. Through comparison between experimental and numerical results, the applicability of the current model to the blast furnace hearth is demonstrated. Furthermore, the simulations are used to visualise the liquid flow patterns within the hearth, which could not be obtained from experiments. This is used to show how experimental and numerical methods can be used in a complementing manner.

2. Methods

2.1. Experimental methods

2.1.1. Model blast furnace hearth

A schematic representation of the model hearth is given in Fig. 1, additional properties are given in Table 1. The main vessel consists of a polycarbonate cylindrical tank with an inner diameter of 190 mm. This tank is placed into the cylindrical MPT sensor array, which is described in Section 2.1.3. The set-up and sensor array are surrounded by a Helmholz coil, which was calibrated to cancel the earth magnetic field.

Deionized water is introduced into the vessel through a flow distributor ring, which directs the flow of water along the inner walls. The liquid is removed through one of the eight available

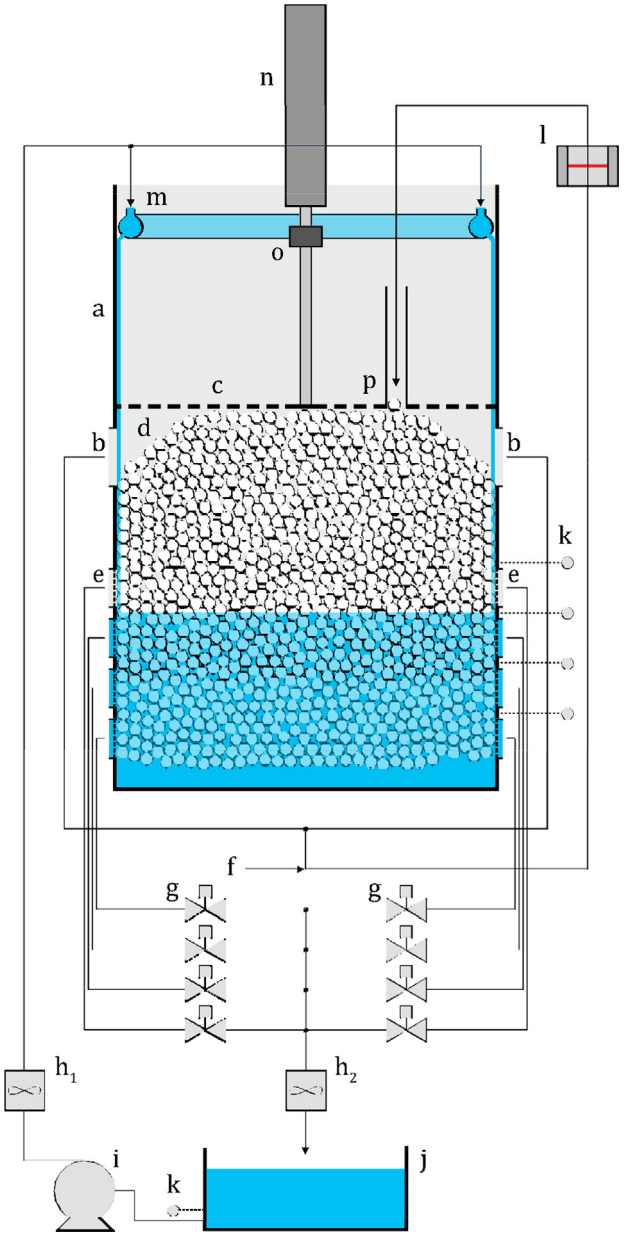

Fig. 1. Schematic representation of the model hearth set-up. Symbols indicate: (a) main vessel, (b) raceway particle outlets (4x), (c) mesh plate, (d) particle bed, (e) tap hole fluid outlets (8x), (f) compressed air, (g) tap hole valves (8x), (h) flow sensors (2x), (i) pump, (j) reservoir, (k) level sensors (5x), (l) particle counter, (m) flow distributor, (n) load cell, (o) particle recycle.

Table 1
Model hearth properties. All heights are measured from the hearth inner bottom.

Property		Value	unit
Hearth inner diameter	D_H	190	mm
Hearth inner height	h_H	300	mm
Tap hole height	h_{th}	25, 50, 75, 100	mm
Tap hole area	A_{th}	134	mm^2
Tap hole hydraulic diameter	D_{th}	3	mm
Raceway height	h_{rw}	165	mm
Number of raceways	N_{rw}	4	–
Raceway diameter	D_{rw}	30	mm
Level sensor height	h_{ls}	45, 70, 95, 120, 140	mm
Water inflow	$\Phi_{v,in}$	0–6	L/min
Particle diameter	d_p	4.5–5.6	mm
Particle density	ρ_p	405	kg/m^3

tap holes, which are located in opposite pairs at 4 different heights and fitted with individual solenoid valves. Each tap hole consists of 19 smaller (3 mm) holes to prevent particles being entrained in the liquid flow. Two flow meters are installed to monitor the outflow and control the inflow, recirculating the tapped water through a tank and pump. Five capacitive level sensors, positioned 20 mm above each tap hole and underneath the raceway level allow for monitoring of the liquid level inside the main vessel.

In order to simulate the weight of the burden above the hearth, a linear actuator is used to apply a force to the particle bed. This force is transferred through a mesh plate, which does not obstruct the liquid flow. A load cell installed between the actuator shaft and the mesh plate allows for control of the force applied to the particle bed. To mimic the combustion of particles in the raceway regions, particles are removed through four outlets. These removed particles are recirculated pneumatically. Before being reinserted through the mesh plate, the recirculated particles are counted by an optical laser gate.

In Table 2, the model blast furnace hearth is compared with a typical industrial blast furnace (Panjkovic et al., 2002; Omori, 1987; Inada et al., 2009; Li et al., 2019; Peacy and Davenport, 1979; Liu et al., 2012) through geometric ratios and dimensionless groups. While a perfect scaling of all physical phenomena is not possible, care has been taken to maintain the balance between particle gravity, buoyancy and the liquid flow, as expressed by the Reynolds, Archimedes and Froude numbers (Re, Ar, and Fr, respectively). The most significant deviation is found in the liquid/solid density ratio (2.5 for the model hearth, instead of 7 for an actual blast furnace), which is mainly limited by the relatively heavy magnetic tracer required for the MPT technique, preventing the use of much lighter particles.

Table 2
Scaling comparison between the model hearth and a typical industrial blast furnace (Panjkovic et al., 2002; Omori, 1987; Inada et al., 2009; Li et al., 2019; Peacy and Davenport, 1979; Liu et al., 2012), where $A_H = \frac{\pi}{4} D_H^2$ is the hearth cross-sectional area, $U_{0,in} = \Phi_{v,in}/A_H$ the superficial inlet velocity, $U_{th} = \Phi_{v,in}/A_{th}$ the outlet velocity, and $\Delta\rho = \rho_l - \rho_p$ and the liquid-solid density difference.

		Blast furnace hearth	Model hearth
	ρ_p/ρ_l	7	2.5
	d_p/D_H	$200 - 400$	$34 - 42$
	h_{rw}/D_H	$0.2 - 0.6$	0.87
	h_{th}/D_H	$0.1 - 0.3$	$0.13 - 0.53$
	A_{th}/A_H	$10^{-5} - 10^{-4}$	$4.6 \cdot 10^{-3}$
Re_H =	$U_{0,in}\rho_l D_H/\mu_f$	$300 - 1500$	$90 - 670$
Re_p =	$U_{0,in}\rho_l d_p/\mu_f$	$2 - 12$	$2 - 20$
Re_{th} =	$U_{th}\rho_l D_{th}/\mu_f$	$5 \cdot 10^4 - 3 \cdot 10^5$	$300 - 2,300$
Ar =	$g d_p^3 \rho_l \Delta\rho/\mu_l^2$	$10^8 - 10^9$	$5 \cdot 10^5 - 1 \cdot 10^6$
Fr =	$U_{0,in}/\sqrt{g d_p \Delta\rho/\rho_p}$	$3 \cdot 10^{-5} - 1 \cdot 10^{-4}$	$10^{-3} - 10^{-2}$

2.1.2. Particle bed

The floating particle bed is composed of hollow alumina shells with a size distribution between 4.5 and 5.6 mm and an apparent density of 405 kg/m^3. These particles are lightweight while providing relatively high degrees of sphericity and mechanical stability. In order to eliminate the effects of surface tension, the particles were treated with a hydrophobic zirconium tetrabutanolate coating. The magnetic tracer consists of a 2.5 mm neodymium magnet encapsulated in a 7 mm polystyrene sphere, resulting in an effective density of 585 kg/m^3 and a magnetic moment of $6.75 \cdot 10^{-3}$ $A{\cdot}m^2$.

2.1.3. Magnetic Particle Tracking

In Magnetic Particle Tracking (MPT), a single magnetic tracer particle is tracked over time through the measurement of the generated magnetic field. This technique has previously been a applied in a wide variety fields, including gas-solid fluidisation (e.g. Richert et al., 2006; Neuwirth et al., 2013; Yang et al., 2017; Köhler et al., 2017; Buist et al., 2017; Mema et al., 2020; Wu et al., 2021). An array of sensors surrounding the set-up captures the magnetic field strength, and reconstruction is applied to obtain the position and orientation of the tracer. The equipment and methods used in this work were described previously by Buist et al. (2014). The sensor array has a cylindrical geometry of inner radius 0.26 m and height 0.45 m, and contains 72 Anisotropic Magnetic Resonance (AMR) sensors.

The sensors measure the magnetic field strength at 1 kHz, which in this work was down-sampled to 1 Hz. This allowed for sufficient noise-reduction to track the relatively small magnet. In order to eliminate any magnetic interference from the moving actuator and switching solenoid valves, the signals from these elements without tracer were correlated with the actuator and valve positions. This was used to obtain a correction signal from the actuator and valve positions during the actual experiments, which was subtracted from the tracer signal before reconstruction. This procedure was found to work well, provided the actuator movement was slow and the solenoid valves were positioned far from the MPT sensor array.

The tracer position is obtained from the magnetic field strength data through an iterative process. By comparison of the measured signal with a theoretical signal corresponding with an initial guess, a series of consecutive guesses is made. This process is repeated until a sufficiently small error between the measured and theoretical signal is obtained. For further details on this reconstruction and its implementation, the reader is referred to the work of Buist et al. (2014).

2.1.4. Experimental procedure

Experiments were conducted in runs of 6 h. During these runs, the controller was programmed to open the selected tap hole when the water level reached the determined upper limit sensor. The liquid was then tapped until the lower limit sensor is reached. The water level therefore constantly alternated between these two switching points. Meanwhile, the water inflow and applied weight were kept constant, such that the particle bed was allowed to move with the alternating liquid level.

Before each experiment, the hearth was filled with the required mass of alumina particles. The MPT sensors were then tared, and the tracer was placed in the centre of the hearth, approximately 1 cm below the bed surface. The mesh plate was then installed and the automatised program initiated. During the experiment, the procedure had to be paused occasionally to manually dislodge small groups (10–20) of particles and to ensure recycled particles were inserted into the bed properly. Care was taken not to disturb the experiment during this operation.

Table 3 provides an overview of the different experiments conducted. In experiments (1–4), the distance between the switching points was kept equal, resulting in an equal length of the tapping cycle. Tap holes at different heights were used, effectively varying the sump depth of the hearth. Contrarily, experiments (1, 5–7) were conducted with equal tap hole heights and low-level switching points, but increasing high-level switching points. This corresponds with a longer tapping cycle and a larger amount of liquid removed per tap. The total bed mass and burden weight were selected such that the bed surface was at the raceway level during the start of the tapping. The burden weight was kept constant except for measurements with the largest two bed sizes, in which the bed was resting on the vessel bottom. To prevent the mesh plate from crushing the particles, the applied force was lowered in these cases.

2.2. Numerical methods

2.2.1. VOF/CFD-DEM

The numerical simulations presented in this work were conducted using the CFDEMcoupling (Goniva et al., 2012) framework, which is based on OpenFOAM and LIGGGHTS (Kloss et al., 2012). Within the unresolved CFD-DEM methodology, a finite volume solver is used to evaluate the fluid flow on a length scale larger than the particle size ($2 \geqslant \Delta x/d_p \leqslant 10$ (Volk et al., 2017)). Particles are treated as discrete entities, and their collisions are resolved through a contact model (Di Renzo and Di Maio, 2004). The interaction between the discrete and continuous phases is established through the momentum coupling, consisting of different force models. In this work, the previously presented liquid-solid momentum coupling is employed (Nijssen et al., 2020), which encompasses drag, lift, virtual mass and Basset history forces. In order to simulate the free surface of the liquid inside the blast furnace hearth, this method is combined with the Volume of Fluid (VOF) methodology (Hirt and Nichols, 1981). This allows for the simulation of an arbitrary number of continuous phases, and thereby enables distinction between the liquid iron phase and the gas phase above it.

In the VOF methodology, transport equations for the volumetric phase fractions ϕ_i in each computational cell are included. The phase-averaged properties such as density and viscosity are established through so-called mixing rules. These averaged properties are then used to solve a single set of momentum equations. This approach is a fairly robust and efficient method for the simulation of multiphase systems (Prosperetti, 2002). Compared to other multiphase CFD methods, a major drawback of the VOF method is the loss of information on the exact location and shape of the interface. Rather than a sharp boundary between phases, a gradient of phase fractions exists, often distributed over multiple cells. This renders the VOF method mainly suited for systems without highly curved interfaces or small features. Various reconstruction methods have been introduced to mitigate this problem (Prosperetti, 2002; Milacic et al., 2019), in which geometric relations are used to reconstruct the location and shape of the sharp interface. In large-scale systems, such as the blast furnace hearth, the diffused interface is a matter of lesser concern, as the interface width and curvature remain small compared to the system size. Therefore, an algebraic VOF method (i.e. without geometric reconstruction) is employed in this work, as it offers a greater computational efficiency. The VOF/CFD-DEM formulation used here is based on the OpenFOAM `interFoam` solver (Rusche, 2002), and was first introduced by Vångö et al. (2018, 2019). The momentum and phase fraction transport equations will not be repeated here. Instead, the reader is referred to the original work of Vångö et al. (2018, 2019).

The wetting behaviour of the liquid and particles was not included in the current model. In the experiments, wetting effects were eliminated through the application of a hydrophobic coating to the particle surface. This is believed to give a more accurate representation of the blast furnace, where gravity dominates over surface tension, as expressed by the Eötvös number $\mathrm{Eo} = \frac{\Delta\rho g d_p^2}{\sigma} \approx 150 \gg 1$. Similarly, wetting effects have been neglected in the simulations presented in this article.

2.2.2. Simulation set-up

A simulation geometry has been created to closely resemble the model blast furnace hearth. The cylindrical domain is decomposed into a hexahedral mesh with cell size $\Delta x = 12.5$ mm, as shown in Fig. 2. The corresponding sizes are taken from the experimental set-up, as given in Table 1. A force-controlled moving wall was used to mimic the weight of the particle bed above the hearth, in a similar fashion as in the experiments. A proportional controller was used to maintain the total burden weight F_B. The raceway regions, which were represented by cut-outs in the hearth wall in the experiments, were represented by thin ($L_{rw} = 3$ mm) cylindrical regions in which particles are removed. No new particles were inserted in the bed during the simulations; the total removed mass ranged between 1% and 15% of the initial bed mass.

Table 4 lists the particle and fluid material properties used in these simulations. The gas and liquid properties are chosen to represent room-temperature air and water, respectively. The Herzian contact model (Di Renzo and Di Maio, 2004) is used to evaluate particle collisions. The particle size is taken uniformly distributed between the sieve mesh sizes used in experiments. The coefficient of restitution, which is used to account for the lubrication forces between particles, has been estimated based on the work of Yang and Hunt (2008). Observing typical liquid and bed velocities, the Stokes number $\mathrm{St} = \frac{d_p \rho_p v}{9 \rho_f \nu_f}$ is expected to lie in the range 1–25. This range corresponding to a typical effective restitution coefficient in the between 0 and 0.5 (Yang and Hunt, 2008), of which 0.3 is used as a representative value.

The tap hole is represented by a 2×2 cells (25×25 mm) patch on the hearth side wall. The tap hole cross-sectional area of the experimental set-up is smaller than the area of this outflow patch. Additionally, the piping and valves present in the flow path (Fig. 1)

Table 3
Overview of conducted experiments. The indicated heights are measured from the hearths inner bottom.

#	Tap hole height	Low-level switch point	High-level switch point	Burden weight	Total bed mass	Liquid inflow rate
1	25 mm	45 mm	70 mm	0.5 N	1.18 kg	0.8 L/min
2	50 mm	70 mm	95 mm	0.5 N	1.11 kg	0.8 L/min
3	75 mm	95 mm	120 mm	2.0 N	0.79 kg	0.8 L/min
4	100 mm	120 mm	140 mm	2.0 N	0.60 kg	0.8 L/min
1	25 mm	45 mm	70 mm	0.5 N	1.18 kg	0.8 L/min
5	25 mm	45 mm	95 mm	0.5 N	1.11 kg	0.8 L/min
6	25 mm	45 mm	120 mm	2.0 N	0.79 kg	0.8 L/min
7	25 mm	45 mm	140 mm	2.0 N	0.60 kg	0.8 L/min

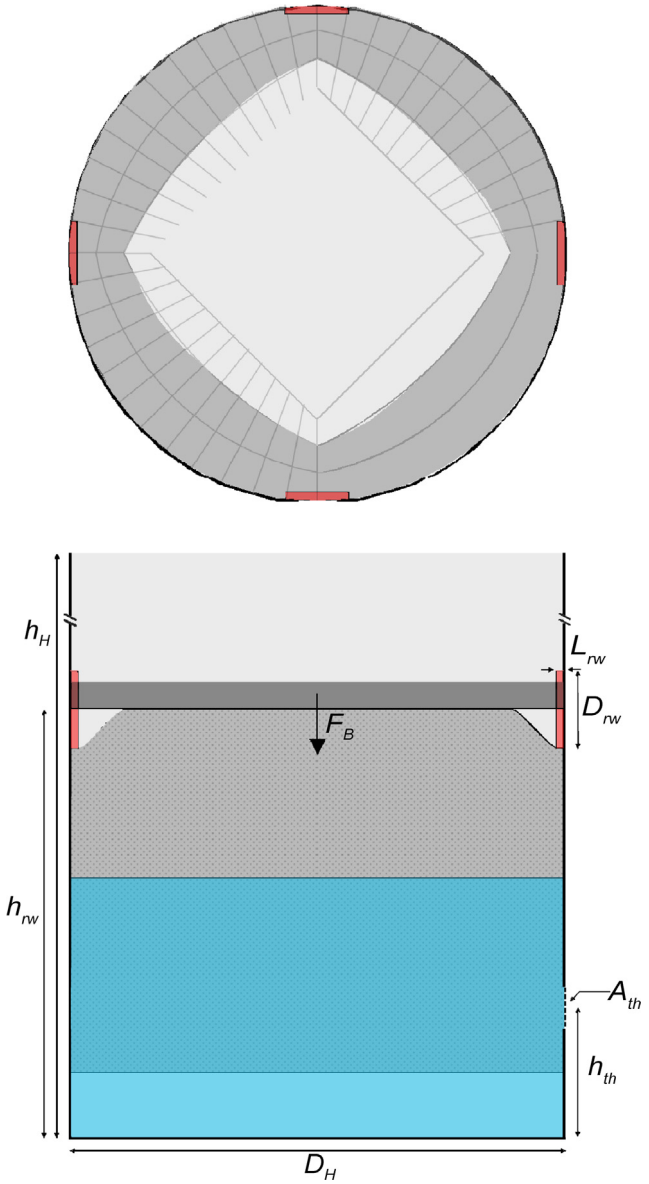

Fig. 2. Schematic representation of the model hearth simulation geometry, top and side views. Particles entering the red raceway areas are removed from the simulation. The position of the horizontal wall is controlled to maintain the burden weight F_B. Sizes are listed in Table 1.

Table 4
Material properties used in simulations. Particle size is uniformly distributed between the given limits. The coefficient of restitution is estimated according to the work of Yang and Hunt (2008).

Property		Value	Unit
Particle size	d_p	4.5–5.6	mm
Particle density	ρ_p	405	kg/m^3
Young's modulus	Y_p	5.0	MPa
Poisson's ratio	ν_p	0.3	–
Coeff. of restitution	e	0.3	–
Coeff. of friction	μ	0.5	–
Coeff. of rolling friction	μ_r	0.2	–
Coeff. of rolling damping	η_r	0.3	–
Liquid density	ρ_l	998	kg/m^3
Liquid viscosity	ν_l	$1.0 \cdot 10^{-6}$	m^2/s
Gas density	ρ_g	1.20	kg/m^3
Gas viscosity	ν_g	$1.51 \cdot 10^{-5}$	m^2/s
Surface tension	σ_{gl}	0.073	N/m

introduce a resistance, influencing the outflow. Both these effects must be accounted for to obtain tapping rates similar to those observed in experiments. The difference in outflow areas was corrected through the porosity boundary condition, as given in Eq. 1. The outflow friction was modelled as a pressure drop over the outflow, given by Eq. 2. Here, $p_0 = 0$ Pa is the environmental pressure and U_{out} the outflow velocity, calculated through the volumetric flow rate (Eq. 3). The coefficient of resistance k_f must be empirically determined. To this end, the drainage rate of the hearth model without any particles was measured, and an appropriate value of $k_f = 10$ was found.

$$\epsilon_{out} = \frac{A_{th}}{A_{out}} \tag{1}$$

$$p_{out} = \frac{1}{2}\langle\rho_f\rangle k_f U_{out}^2 + p_0 \tag{2}$$

$$U_{out} = \frac{\Phi_{V,out}}{A_{th}} \tag{3}$$

The opening and closing of the tap hole valve in the experiments was simulated through switching of the outlet boundary conditions between wall conditions and the outflow conditions described in the previous paragraph. Much like in experiments, this switching was controlled by the rising and falling liquid level. During the simulation, the liquid level was evaluated through Eq. 4. High and low-level switch points were defined, at which the tap hole was opened and closed, respectively. To this end, simulations were conducted in short (5 s) consecutive runs. After each run, the liquid level was compared with the switch points, and the boundary conditions set accordingly. The simulation was then continued using the updated conditions.

The list of simulations conducted in this study is identical to the list of experiments presented in Table 3. All simulations were conducted for a total of 26 tapping and filling cycles, the first of which was omitted from the analysis to eliminate initialisation effects.

$$h_l = \frac{\sum_{i=0}^{N_{cells}} \phi_{L,i} V_i}{\frac{\pi}{4} D_H^2} \tag{4}$$

3. Results and discussion

3.1. Experimental results

Fig. 3 shows the state of the bed and the liquid level for the experiments listed in Table 3, at the start (left bar) and end of tapping (right bar). In this figure, the vertical displacements of both the bed and the liquid level are shown, which are not equal as the bed reaches a sitting state in many experiments. The liquid level was obtained from the level sensors, while the bed position is derived from the actuator position and the measured bed height. The bed level in the upper position was kept approximately at the raceway level. At the lowest (experiment 1) and second lowest (experiments 2 and 5) upper liquid level, no to little coke-free space under the bed was found, while at the higher liquid levels, where buoyancy is more dominant over the bed weight and added burden weight, a significant coke-free space is observed. Experiments (1–4) exhibit an approximately equal difference between the upper and lower level, with increasing tap hole height. Conversely, experiments (1, 5–7) show a similar lower state of the bed, with an increasing liquid level at the upper state.

During experiments with a floating bed state, the lower surface of the bed was observed to remain mostly flat. In previous experiments by Shibata et al. (1990), the angle of the lower surface was

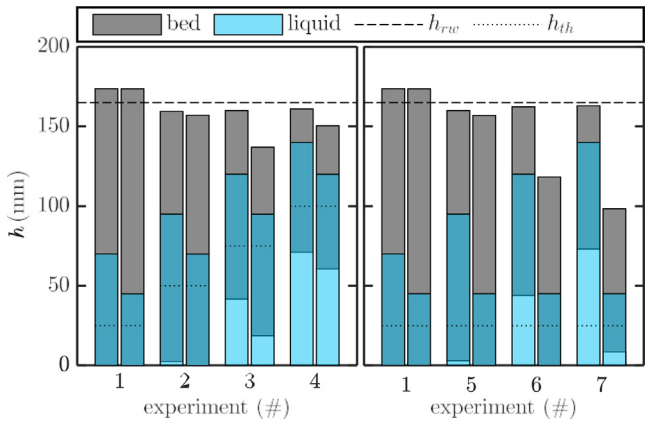

Fig. 3. Bed and liquid level positions for all experiments (Table 3) at the start (left bar) and end of tapping (right bar). Experiments (1–4) (left) were performed with equal tapping cycle length and increasing tap hole height, whereas experiments (1, 5–7) (right) were performed with equal tap hole height and increasing tapping cycle length. Liquid (light blue) level is obtained through level sensors, the bed (grey) position is derived from the actuator position and measured bed height. Dark blue represents the area where the bed is submerged in the liquid. Height of the raceways and tap holes are indicated.

found to vary between the horizontal and the particle angle of repose, increasing with increasing upper liquid level. However, these experiments were conducted in a 2D slot geometry, introducing significant wall friction to the system. As the current work is conducted using a full 3D geometry, the influence of wall friction is much lower, resulting in a more flat state of the lower bed surface.

3.2. Particle movement

Per example, the trajectory of the tracer during experiment 6 is visualised in Fig. 4, for the three different tracer starting positions. The corresponding radial and axial positions are plotted over time in Fig. 5. The tracer can clearly be seen to follow the vertical oscillation of the liquid level (seen in Fig. 3), but no net vertical movement of the tracer is observed. This contradicts the findings of Takahashi et al. (1996), who found a net downward movement underneath the raceway regions in their experiments. In their work, solids were discharged from the bottom of the hearth, thereby significantly altering the solids flow patterns. Presumably, in our work vertical migration is only driven by result of the oscillating bed motion and particle discharge, and only happens on a time-scale longer than the current experimental runs.

The trajectories recorded close to the wall and halfway between the wall and bed centre clearly show a slow horizontal migration of the particle, towards the vessel wall and, ultimately, the raceway regions. This can be observed both from the start and end positions in Fig. 4 and the sloped lines in Fig. 5. In the bed centre, a slight horizontal movement of the tracer is found during the tapping, but no long-term migration is found. This movement was previously observed in experiments (Takahashi and Kawai, 2001; Kawai and Takahashi, 2004) and simulations (Kawai and Takahashi, 2004). These authors identified two mechanisms for the deadman renewal; particles being either pushed into the active flowing layer above the deadman or migrating through the deadman towards the raceways in a zig-zag motion. The current findings show that the migration mechanism is present even in the absence of a flowing layer, confirming the assumption that particle migration is mainly driven by the oscillating liquid level and the resulting vertical bed motion (Takahashi and Kawai, 2001; Kawai and Takahashi, 2004).

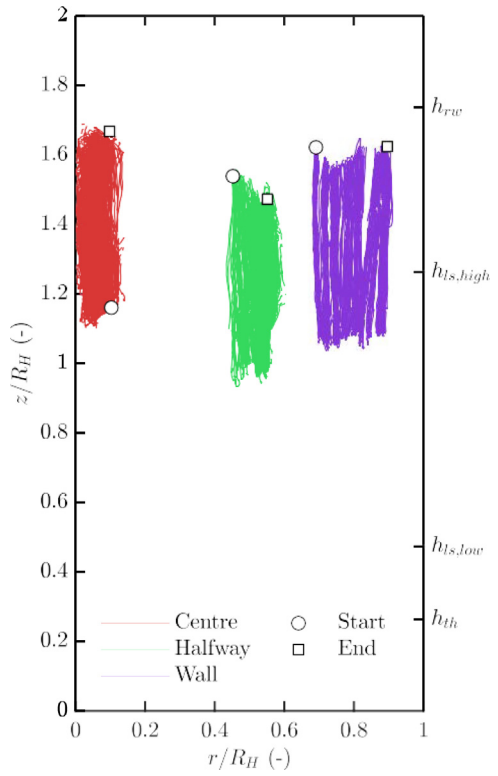

Fig. 4. Trajectories of the tracer particle during experiment 6 (Table 3) for three different tracer starting positions. Experiment duration was 6 h per run. Symbols indicate the start and end of the trajectory. Height of the tap hole, liquid level switching points and raceways are indicated. The corresponding radial and axial positions over time are shown in Fig. 5.

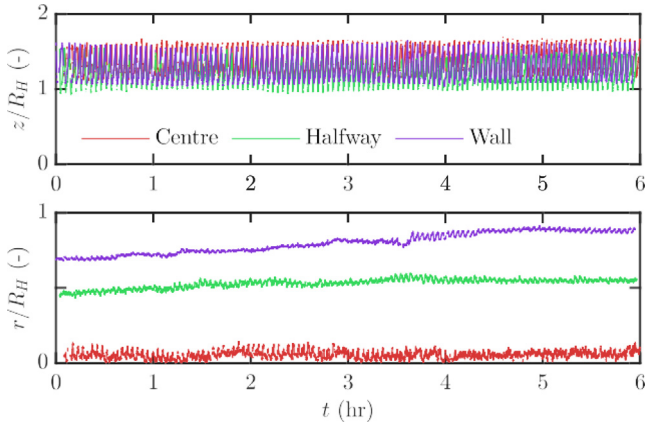

Fig. 5. Radial and axial position of the tracer particle over time during experiment 6 (Table 3) for three different tracer starting positions, corresponding to the trajectories in Fig. 4.

The mean vertical amplitudes of the tracer movement, coke-free space height and liquid level are shown in Fig. 6. The vertical movement of the tracer is found to be closely related to the overall movement of the bed, indicated by the coincidence of the tracer and coke-free space amplitudes. It can be concluded that particles in the bed have negligible vertical mobility during the tapping cycle. The bed movement is coupled to the liquid level movement through the force balance between buoyancy, bed weight and burden weight added through the mesh plate (Fig. 1). The amplitudes in Fig. 6 correspond with the bed positions in Fig. 3, showing how

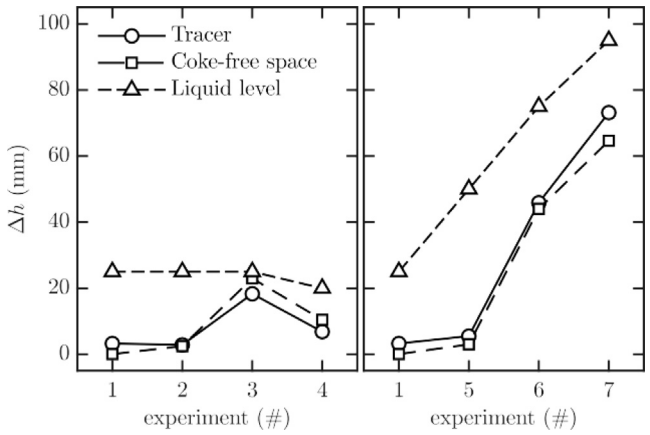

Fig. 6. Mean vertical amplitudes the tracer particle movement, coke-free space height and liquid level. Experiments (1–4) (left) represent increasing tap hole height, experiments (1, 5–7) (right) represent increasing tapping cycle length. The parameters used in each experiment are detailed in Table 3.

the deadman can be in fully sitting, partially floating, or fully floating states.

In Fig. 5, it is shown that particles in the upper section of the deadman can undergo a slow radial migration through the bed. The rate of this migration mechanism is detailed in Fig. 7, which shows the mean radial displacement of the tracer measured at different positions within the bed. A distinct difference is found between the core of the bed and the regions close the walls and raceways. This separation is represented by the dashed line. The top figure shows that no radial movement is found in case of a fully sitting deadman. Only when there is a vertical movement of the bed during the tapping cycle, a radial movement of the individual particles is observed in the core of the bed. Little difference is found between the two floating deadman cases with equal tapping cycle lengths (experiments 3 and 4), indicating that the height of the coke-free space does not directly influence the particle motion.

The bottom figure of Fig. 7 shows the influence of the tapping cycle length on the radial displacement of particles. Even though all experiments were conducted with equal liquid production rates, the length of the tapping cycle significantly influences the particle movement. A larger amplitude of the vertical bed movement is found to increase radial migration rate, as was previously suggested by DEM simulations (Kawai and Takahashi, 2004). Furthermore, the radial movement is found to vanish in the bed centre, as would be expected from the radial symmetry of the system.

A strong increase of radial velocity is found near the raceway regions, which does not appear to scale with the tapping cycle length as the migration within the core of the bed does. Rather, in this region, particle movement is strongly influenced by the removal of particles in the raceway regions. This is further illustrated in Section 3.3.

3.3. Particle discharge

During the experiments, particles removed from the hearth in the raceway regions were counted using an optical gate sensor (Fig. 1, l), and pneumatically recycled to the top of the bed. Fig. 8 shows the measured average particle recycle rate for each experiment. Similarly to the radial particle movement measured through MPT, the particle recycle rate was observed to strongly depend on the vertical movement of the bed. However, the recycle rate was found to also strongly depend on the feedback controller governing the movement of the mesh plate. A small under-shoot or over-shoot of the plate movement at the higher bed position, resulting from the combination of experimental conditions and the controller gain settings, significantly influenced the rate at which particles entered the raceway openings. This is evident from the non-monotonous trend in the right-hand side figure of Fig. 8. While this makes analysis of the recycle rate in itself precarious, comparison of Figs. 7 and 8 clearly shows that the radial movement of particles close to the raceway zones is directly connected to the rate at which particles are removed.

Simulations conducted by Kawai and Takahashi (2004) have shown that entry of particles from the deadman into the raceway zones only occurs when the deadman is in its highest floating state i.e. just before and after the opening of the tap hole. Fig. 9 shows the particle recycle rate averaged over the tapping and filling cycle. In this figure, the central point $t = 0$ corresponds with the opening of the tap hole. The total cycle time varied between 30 s for the shortest tapping cycle, and 250 s for the longest. Indeed, particles are found to enter the raceway openings only when the liquid level and bed are in their highest positions, indicating that renewal of the deadman particles is concentrated around this moment within the tapping cycle.

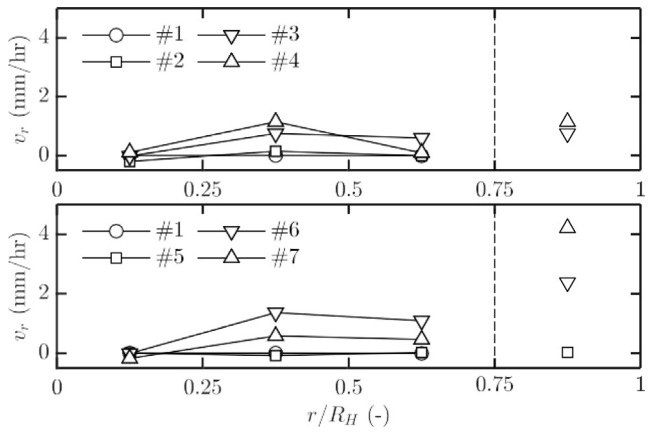

Fig. 7. Velocity of radial migration plotted over the bed radius. Experiments (1–4) (top) represent increasing tap hole height, experiments (1, 5–7) (bottom) represent increasing tapping cycle length. The parameters used in each experiment are detailed in Table 3. The dashed line represent the separation between the bulk and wall regions, where significantly differing behaviour is found.

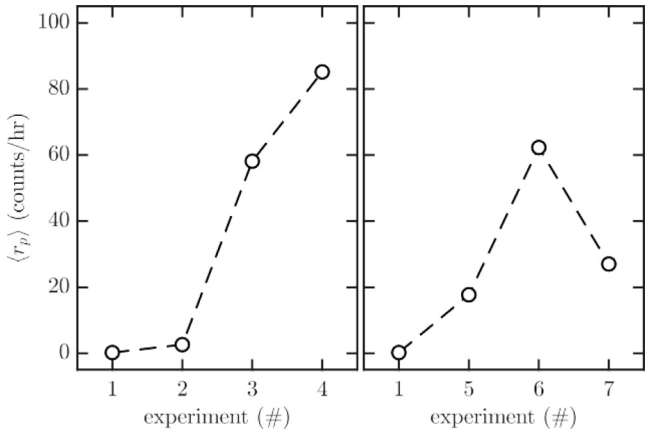

Fig. 8. Mean particle recycle rates measured with the optical gate sensor (Fig. 1, l). Experiments (1–4) (left) were performed with equal tapping cycle length and increasing tap hole height, whereas experiments (1, 5–7) (right) were performed with equal tap hole height and increasing tapping cycle length. The parameters used in each experiment are detailed in Table 3.

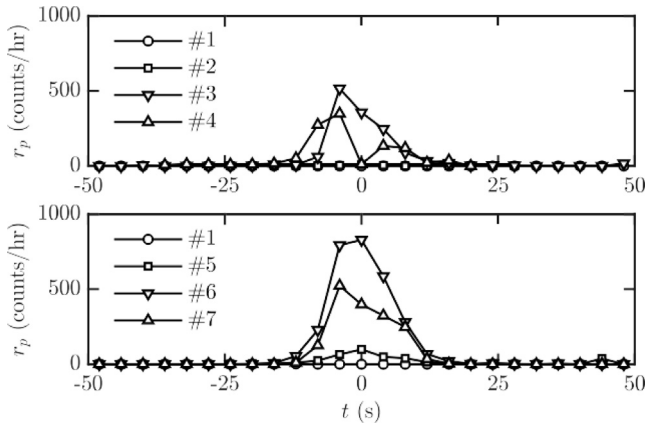

Fig. 9. Particle recycle rates measured with the optical gate sensor (Fig. 1, l) throughout the tapping and filling cycle. $t = 0$ corresponds with the opening of the tap hole. Experiments (1–4) (top) represent increasing tap hole height, experiments (1, 5–7) (bottom) represent increasing tapping cycle length. The parameters used in each experiment are detailed in Table 3.

3.4. Liquid tapping

Aside from measurement of bed and particle movement, the liquid flow rate during tapping was measured using a flow sensor (Fig. 1, h_2). Fig. 10 shows the probability density function of the mean flow rate during tapping. As experiments (1–4) were conducted with an equal tapping cycle length (i.e. difference between high and low level switching points), but increasing coke-free space height, the top figure of Fig. 10 shows the influence of coke-free space on the mean tapping velocity. Clearly, a bimodal distribution of the tapping rates is found, with no obvious influence of the coke-free space. In previous experiments, He et al. (2012) found that the coke-free space mainly influences the gas break-through and iron/slag tapping ratio, which were not explicitly measured in this study. However, Nouchi et al. (2003) observed that the tapping rate was strongly dependent on the bed state directly in front of the tap hole. This can be used to explain the bimodal distribution found in the current work, considering a state in which particles partially block the tap hole, and a state in which the tap hole cross-section is particle-free. This is supported by the fact that only the higher tapping rate is found in cases where vertical bed movement disturbs the packing in front of the tap hole.

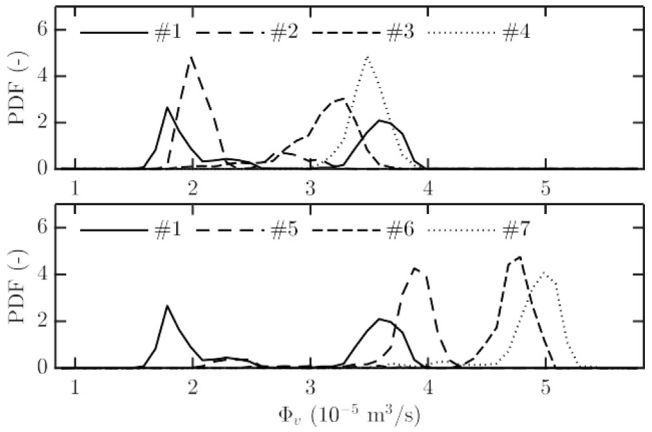

Fig. 10. Mean tapping rate obtained from the outflow sensor (Fig. 1, h_2). Experiments (1–4) (left) represent increasing tap hole height, experiments (1, 5–7) (right) represent increasing tapping cycle length. The parameters used in each experiment are detailed in Table 3.

Experiments (1, 5–7) were conducted with increasing tapping cycle length, and the mean tapping rate is found to increase accordingly. As these cases exhibit larger vertical bed movement, no bimodal distribution is found for longer tapping cycles. Furthermore, a significant increase in tapping rate is found between experiments 5 and 6. This corresponds with the point at which the particle bed clears the tapping hole at its highest position (as shown in Fig. 3), providing the liquid with a free path towards the tap hole.

In conclusion, the mean tapping rate is found to be mainly influenced by the state of the coke bed directly in front of the tap hole, where the liquid velocity is highest and therefore flow resistance is most significant. No direct influence of the coke-free space height on the tapping rate is found in these experiments. However, the vertical motion on the bed can influence the tapping rate through the disturbance of the packing directly in front of the tap hole, or possibly even completely clearing it. In such cases, an increased tapping rate was found, stemming from the decreased flow resistance in front of the tap hole.

3.5. Numerical results

The experimental results presented in Section 3.1 were reproduced using VOF/CFD-DEM simulations. Fig. 11 shows snapshots from simulation cases 1 and 4, taken at the onset of tapping. The particle bed and the liquid level are indicated, showing the sitting and floating deadman states previously observed in experiments. A complete overview of the simulation cases is provided by Fig. 12, which shows the bed and liquid level positions for all cases at the start and end of the tapping cycle. Here, the liquid level is calculated through Eq. 4, whereas the bed position is defined by the heights between which 99% of the bed mass is contained.

When comparing the numerical results in Fig. 12 with the experimental results presented in Fig. 3, a close correspondence for the bed position can be observed. The transition from the sitting (case 1) to the partially floating (cases 2, 5–7) and fully floating (cases 3–4) states is well-predicted by the simulations, indicating that the current VOF/CFD-DEM method is well-suited for simulation of such floating particle beds. This is confirmed by the quantitative comparison provided in Fig. 13. In this figure, the amplitude of the coke-free space height is shown from both experimental and numerical studies. Deviations from the experiments, most notably in case 3, can be explained by a difference in behaviour of the force-controlled plates in experiments and simulations. Small differences in the controller gain can impact the bed motion significantly, both in experiments and simulations. However, the overall movement of the bed due to the tapping and filling cycle is found to be captured very well by the VOF/CFD-DEM model.

In Fig. 14, the liquid level (Eq. 4) and volumetric in and outflow rates measured in case 1 are shown over time for 6 complete tapping cycles. The pre-determined level switching points are indicated, and the boundary conditions can be seen to switch accordingly. A constant inflow rate is maintained, whereas the outflow is enabled only when the liquid level has reached the high level switching point. Furthermore, the observed outflow rate lies within the same range observed in experiments, $(2–4) \cdot 10^{-5}$ m^3/s (Fig. 10). From these results, it can be concluded that the current method of switching boundary conditions is well-suited for the simulation of the alternating blast furnace tapping.

In the analysis of the experimental results, special attention was given to the slow migration of particles through the coke bed. Fig. 15 shows particle trajectories recorded in simulation case 6, similar to the experimental trajectories previously presented in Fig. 4. As in the experiments, the tracked particles are chosen in the vertical plane through the raceways. While CFD-DEM simula-

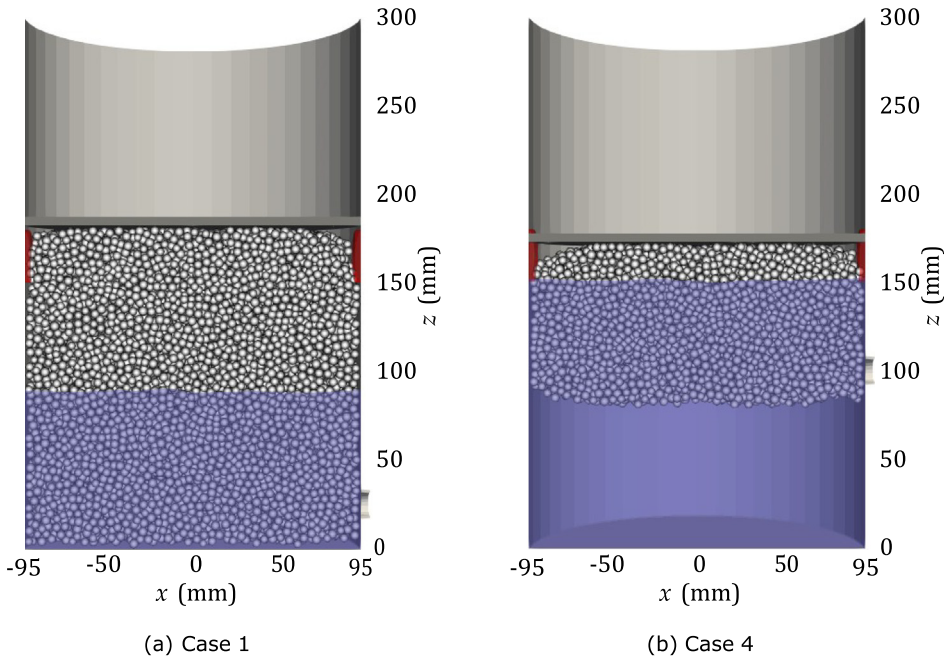

Fig. 11. Cross-sectional views of simulation cases 1 and 4 (Table 3). The particle bed, force-controlled wall and liquid level are shown. The disk-shaped raceway zones are indicated in red. All snapshots are taken at the onset of tapping.

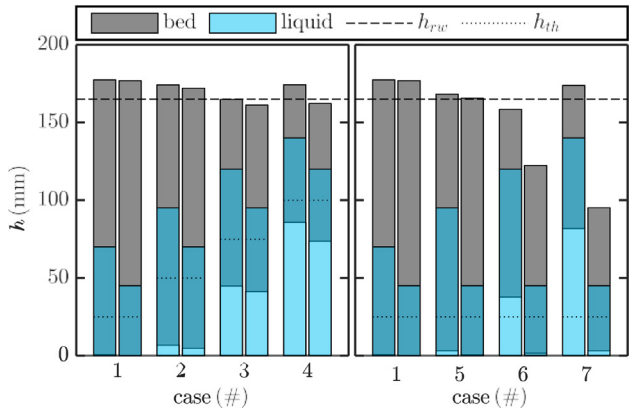

Fig. 12. Bed and liquid level positions for all simulations (Table 3) at the start (left bar) and end of tapping (right bar). Cases (1–4) (left) represent an equal tapping cycle length and increasing tap hole height, whereas cases (1, 5–7) (right) were performed with equal tap hole height and increasing tapping cycle length. The liquid (light blue) level is calculated through Eq. 4, the bed (grey) position is defined by the heights between which 99% of the bed mass is contained. Dark blue represents the area where the bed is submerged in the liquid. Height of the raceways and tap holes are indicated.

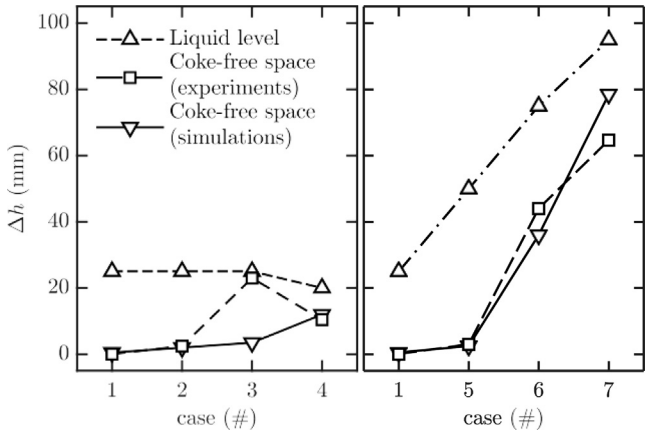

Fig. 13. Comparison between coke-free space height amplitudes and liquid level obtained from experiments and simulations. The parameters used in each experiment and simulation are detailed in Table 3 and Table 3, respectively.

tions allow for the simultaneous tracking of all particles within the domain, the duration of the tracking is limited by the computational time. The trajectories in Fig. 15 represent 25 full filling and tapping cycles, whereas the 6-h experiments in Fig. 4 cover around 110 full cycles. Nevertheless, it is clear from Fig. 15 that particle migration occurs within the simulations. Both inward and outward migration is observed, depending on the location within the bed. A relatively rapid migration is found near the raceway regions, where the removal of particles increases the local mobility. Furthermore, increased mobility is found in the lower section of the hearth, close to the free lower surface of the bed. It is expected that the obtained migration pattern is highly dependent on material properties and set-up dynamics, both in experiments and simulations. Calibration of the simulation parameters in order to obtain a perfect

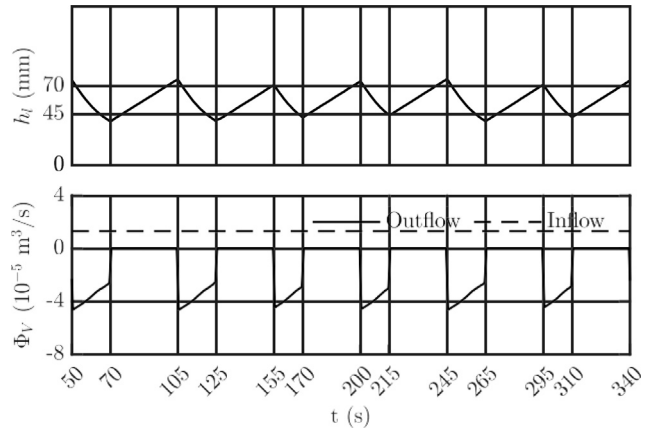

Fig. 14. Liquid level (top, Eq. 4), and flow rates (bottom) obtained from simulation case 1 (Table 3). Liquid level switch points and switching times are indicated.

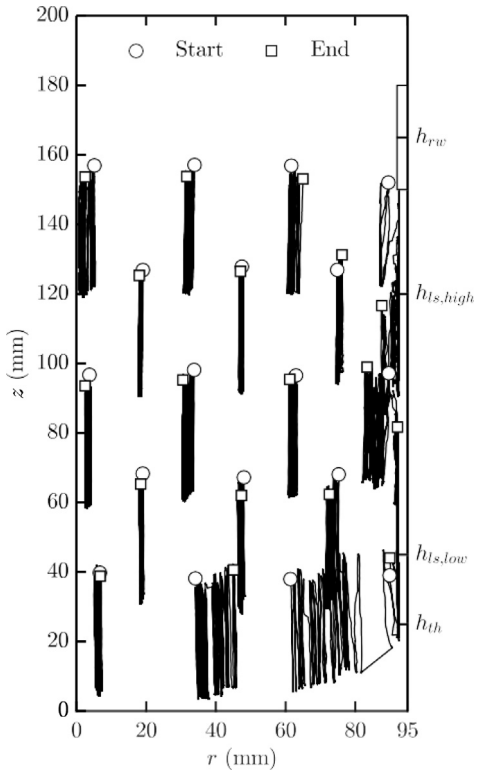

Fig. 15. Particle trajectories recorded in case 6 (Table 3), spanning 4 tapping and filling cycles. All trajectories are captured in a vertical plane through the raceway regions. Height of the tap hole, liquid level switching points and raceways are indicated. The disk-shaped raceway zone is represented by the grey rectangle.

correspondence between experimental and numerical results is considered outside the current scope, as it provides little additional insight in the industrial blast furnace operation.

While long-term particle migration is difficult to capture with simulations over experiments, the numerical route has the added advantage of simultaneously providing information on the particle motion and the liquid flow. Per illustration, Fig. 16 shows the time-averaged liquid flow during tapping in cases 1 and 3. The streamlines and background colour show the flow pattern and magnitude, whereas the yellow and grey lines show the liquid level and position, respectively. In the case of a sitting deadman (case 1), a mostly uniform flow pattern is observed, where the liquid flows through the particle bed. In case of a floating deadman (case 3), however, a clear distinction is observed between liquid moving through the bed and liquid moving underneath it. Liquid drawn from the surface close to the tap hole moves directly through the particle bed towards the tap hole. On the opposite side of the hearth, liquid moves through the coke bed into the low-resistance coke-free space, and then moves upwards again towards the tap hole. This pattern creates an increased-velocity zone directly underneath the tap hole, possible increasing the mechanical and thermal stress on the walls in a real blast furnace. This illustrates how significantly the presence of a coke-free space affects the flow pattern during blast furnace tapping, and thereby influences the erosion process of the hearth lining.

4. Conclusions

In this work, a small cold-flow blast furnace hearth model was presented, which has been used to study coke behaviour within the deadman of the blast furnace. The movement of an individual tracer particle was measured using Magnetic Particle Tracking, which allows for particle tracking in a full 3D and opaque system. The design of the model hearth was based on a scaled-down version of a typical industrial blast furnace, maintaining geometric and physical ratios as much as possible. The liquid hot metal and deadman coke particles were simulated with water and hollow alumina shells, respectively.

Long-term experiments were conducted with increasing hearth sump depth and increasing length of the tapping cycle, while maintaining equal liquid production rates. For cases with a larger liquid hold-up, the bed was observed to float, creating a coke-free space underneath it. In such cases, the lower surface of the bed was found to remain mostly flat. From MPT results, the trajectory of the tracer was visualised throughout the experiments. The vertical motion of the tracer was found to follow the motion of the

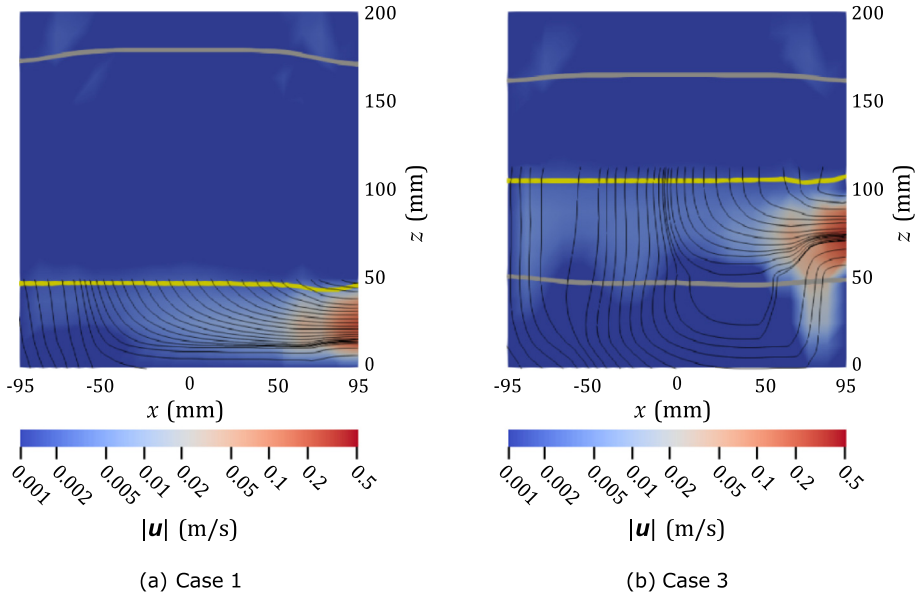

Fig. 16. Time-averaged liquid flow during tapping in cases 1 and 3 (Table 3), represented in the vertical plane through the tap hole. Streamlines indicate the flow pattern, colours represent the velocity magnitude. The yellow line indicates the liquid free surface, the grey lines the upper and lower bed surfaces.

bed as a whole, with no appreciable vertical migration of the particles on the time-scale of the experiments.

Horizontally, the particles were observed to slowly migrate outwards, towards the raceway regions. No net migration was found in the centre of the bed, further outwards the migration rate increased proportionally with the amplitude of the vertical bed motion. This deadman renewal mechanism is driven by the vertical motion of the bed due to buoyancy, as no actively flowing particle layer was present in these experiments. Close to the raceway regions, the radial migration rate increased, with the total rate determined by the particle discharge rate. Furthermore, discharge of particles from the deadman was found to happen only just before and after the opening of the tap hole, indicating that deadman renewal is concentrated around this moment.

Lastly, the tapping rate from the model hearth was analysed. When the total tapped volume was kept equal, a bimodal distribution of tapping rates was found. This is most likely caused by the state of the bed directly in front of the tap hole, either blocking parts of it or keeping the tap hole cross-section free of particles. Only the higher tapping rate corresponding to this second state was observed whenever vertical motion of the bed was present, as the bed motion continually disturbs the packing in front of the tap hole. In the current experiments, no direct influence of the coke-free space height on the tapping rate was found. For longer tapping cycles, the higher average liquid level caused an increase in the average tapping rate. An additional sudden increase was found at the point where the floating bed completely clears the tap hole, stemming from the reduced flow resistance in front of the tap hole.

In addition to the experimental work, the VOF/CFD-DEM model developed by Vångö et al. (2018) was combined with the complete liquid-solid momentum coupling by Nijssen et al. (2020), and used to replicate the experimental results. A simulation set-up was developed, in which the laboratory-scale blast furnace hearth model was reproduced. Special care was taken in the treatment of the tap hole, for which frictional losses and the level-controlled opening and closing sequence were incorporated. The implemented dynamic boundary conditions were found to accurately describe the alternating tapping and filling of the hearth, as well as the flow rate during tapping.

From comparison of the bed position and movement, it was concluded that the VOF/CFD-DEM model accurately predicts the (partial) floating and sitting behaviour of the deadman. The vertical amplitude of the bed position during the tapping cycle showed good correspondence between experiments and simulations. The behaviour of the force-controlled wall used to simulate the weight of the burden above the hearth was observed to be of significant influence on the bed motion. It is therefore recommended to rigorously define this added weight in future numerical work.

In correspondence with the experimental work, individual deadman particle trajectories were visualised from the simulation results. In the 6-h experiments long-term outward radial migration of particles was found to occur. while in the simulations both inward and outward migration of particles was observed. In both cases, the obtained migration pattern is likely governed by material properties and set-up dynamics, and might therefore not be completely representative of the full-scale industrial blast furnace. Due to the slow nature of the migration process, resolving its mechanisms and patterns in simulations is computationally expensive. Novel advanced methods such as recurrence CFD (Lichtenegger et al., 2017) can be applied for more efficient simulation of the slow mechanisms within the system.

While experiments provided more long-term information on the particle behaviour, the simulations allowed for simultaneous evaluation of the particle movement and liquid flow. Flow patterns during sitting and floating deadman simulations were compared to demonstrate the significance of the coke-free space. When a coke-free space was present, the liquid opposite the tapping zone was observed to flow underneath the coke bed and rise towards the tap hole, creating a high-velocity region directly underneath it. This shows that the coke bed shape significantly influences the flow pattern, and thereby the erosion processes within the hearth.

In conclusion, the presented VOF/CFD-DEM model and hearth simulation set-up were found to be in good shape for the simulation of the blast furnace hearth. The force balance on the floating or sitting bed is accurately captured, and the simultaneous evaluation of solid and liquid movement provides valuable information on the mutual interaction between both phases.

5. Outlook

The results presented in this work offer many interesting opportunities for future research. According to the results of Kawai and Takahashi Takahashi and Kawai (2001),Kawai and Takahashi (2004), two mechanisms for deadman renewal exist aside the coke dissolution; particles either leave the deadman and join the actively flowing layer towards the raceways or undergo a slow outward horizontal migration. In the current set-up, only this second mechanism was considered. For more realistic simulation of the deadman renewal, it would be beneficial to incorporate both mechanisms into the set-up design. To accomplish this in experiments, the total discharge rate from the raceways must be placed under user control, for example by use of screw extractors.

Additionally, the current design allows for further in-depth investigation of the blast furnace hearth. In the numerical results presented here, significant particle movement was observed deep in the hearth. This was not yet investigated experimentally, and will provide an interesting future study. In this work, both the liquid production rate and burden weight were kept constant. It is expected that both these parameters significantly impact the particle migration rate, and thereby influence the deadman renewal rate. Also the hearth geometry can play a significant role in the deadman behaviour Liu et al. (2012). In the current work, only the sump depth was varied. In future work, the total hearth depth could be varied through blocking of the lower hearth section.

While the current work provides interesting results on a laboratory scale, much remains unknown about the scalability of these results. As experiments on an industrial scale are infeasible for practical reasons, numerical methods can be used to bridge this gap. This study has shown that the VOF/CFD-DEM method is well-suited for simulation of the dynamics of three-phase systems such as the blast furnace hearth, especially since it considers the motion of both the particle and fluid phases. In future work, high-performance computing (HPC) will be used to scale up this model towards the industrial scale. It will then be used to gain insight in the full-scale behaviour of the blast furnace hearth. Additionally, the model can be extended with heat and mass transfer calculations, in order to study the thermal and chemical processes within the furnace.

Declaration of Competing Interest

The authors declare that they have no known competing financial interests or personal relationships that could have appeared to influence the work reported in this paper.

Acknowledgements

The authors would like to thank Tata Steel Europe for their financial support for this project. This research was carried out under project number S16046 in the framework of the Partnership

Program of the Materials innovation institute M2i (www.m2i.nl) and the Technology Foundation TTW, which is part of the Netherlands Organisation for Scientific Research (www.nwo.nl).

References

Adema, A.T., 2014. DEM-CFD Modelling of the Ironmaking Blast Furnace (Ph.D. thesis). Delft University of Technology.

Adema, A.T., Yang, Y.X., Boom, R., 2010. Discrete Element Method-Computational Fluid Dynamic Simulation of the Materials Flow in an Iron-making Blast Furnace. ISIJ Int. 50, 954–961. https://doi.org/10.2355/isijinternational.50.954.

Andreev, K., Louwerse, G., Peeters, T., van der Stel, J., 2017. Blast furnace campaign extension by fundamental understanding of hearth processes. Ironmaking Steelmaking 44, 81–91. https://doi.org/10.1080/03019233.2016.1154716.

Ariyama, T., Natsui, S., Kon, T., Ueda, S., Kikuchi, S., Nogami, H., 2014. Recent progress on advanced blast furnace mathematical models based on discrete method. ISIJ Int. 54, 1457–1471. https://doi.org/10.2355/isijinternational.54.1457.

Austin, P.R., Nogami, H., Yagi, J.i., 1997. A Mathematical Model of Four Phase Motion and Heat Transfer in the Blast Furnace. ISIJ Int. 37, 458–467. https://doi.org/10.2355/isijinternational.37.458. http://www.jstage.jst.go.jp/article/isijinternational1989/37/5/37_5_458/_article.

Bambauer, F., Wirtz, S., Scherer, V., Bartusch, H., 2018. Transient DEM-CFD simulation of solid and fluid flow in a three dimensional blast furnace model. Powder Technol. 334, 53–64. https://doi.org/10.1016/j.powtec.2018.04.062.

Buist, K.A., van der Gaag, A.C., Deen, N.G., Kuipers, J.A.M., 2014. Improved magnetic particle tracking technique in dense gas fluidized beds. AIChE J. 60, 3133–3142. https://doi.org/10.1002/aic.14512. http://doi.wiley.com/10.1002/aic.14512 http://arxiv.org/abs/physics/0201037.

Buist, K.A., Jayaprakash, P., Kuipers, J.A.M., Deen, N.G., Padding, J.T., 2017. Magnetic particle tracking for nonspherical particles in a cylindrical fluidized bed. AIChE J. 63, 5335–5342. https://doi.org/10.1002/aic.15854.

Cundall, P., Strack, O., 1979. A discrete numerical model for granular assemblies. Geotechnique 1, 47–65.

Di Renzo, A., Di Maio, F.P., 2004. Comparison of contact-force models for the simulation of collisions in DEM-based granular flow codes. Chem. Eng. Sci. 59, 525–541. https://doi.org/10.1016/j.ces.2003.09.037.

Dong, X., Yu, A., Yagi, J.i., Zulli, P., 2007. Modelling of Multiphase Flow in a Blast Furnace: Recent. ISIJ Int. 47, 1553–1570.

Fan, Z., Igarashi, S., Natsui, S., Ueda, S., Yang, T., Inoue, R., Ariyama, T., 2010. Influence of Blast Furnace Inner Volume on Solid Flow and Stress Distribution by Three Dimensional Discrete Element Method. ISIJ Int. 50, 1406–1412. https://doi.org/10.2355/isijinternational.50.1406. http://joi.jlc.jst.go.jp/JST.JSTAGE/isijinternational/50.1406?from=CrossRef.

Feng, Y.Q., Pinson, D., Yu, A.B., Chew, S.J., Zulli, P., 2003. Numerical Study of Gas-Solid Flow in the Raceway of a Blast Furnace. Steel Res. Int. 74, 523–530. https://doi.org/10.1002/srin.200300229.

Goniva, C., Kloss, C., Deen, N.G., Kuipers, J.A.M., Pirker, S., 2012. Influence of rolling friction on single spout fluidized bed simulation. Particuology 10, 582–591. https://doi.org/10.1016/j.partic.2012.05.002.

He, Q., Evans, G., Zulli, P., Tanzil, F., 2012. Cold model study of blast gas discharge from the taphole during the blast furnace hearth drainage. ISIJ Int. 52, 774–778. https://doi.org/10.2355/isijinternational.52.774.

Hirt, C.W., Nichols, B.D., 1981. Volume of fluid (VOF) method for the dynamics of free boundaries. J. Comput. Phys. 39, 201–225. https://doi.org/10.1016/0021-9991(81)90145-5. arXiv:0924-0136(97)00224-0.

Inada, T., Kasai, A., Nakano, K., Komatsu, S., Ogawa, A., 2009. Dissection Investigation of Blast Furnace Hearth-Kokura No. 2 Blast Furnace (2nd Campaign). ISIJ Int. 49, 470–478. https://doi.org/10.2355/isijinternational.49.470.

Jimenez, J., Mochón, J., Formoso, A., Sainz De Ayala, J., 2000. Burden distribution analysis by digital image processing in a scale model of a blast furnace shaft. ISIJ Int. 40, 114–120. https://doi.org/10.2355/isijinternational.40.114.

Kawai, H., Takahashi, H., 2004. Solid Behavior in Shaft and Deadman in a Cold Model of Blast Furnace with Floating-Sinking Motion of Hearth Packed Bed Studied by Experimental and Numerical DEM Analyses. ISIJ Int. 44, 1140–1149. URL file://hermes26/SCC/CFD/Literature CFD/Blast Furnace/isij441140 Kawai and Takahashi 2004 Solid Behavior in Shaft and Deadman in a Cold Model of Blast Furnace with Floating-Sinking Motion of Hearth Packed Bed Studied by Experimental and Numerical DEM Analy, doi: 10.2355/isijinternational.44.1140.

Kloss, C., Goniva, C., Hager, A., Amberger, S., Pirker, S., 2012. Models, algorithms and validation for opensource DEM and CFD-DEM. Prog. Comput. Fluid Dyn. Int. J. 12, 140. https://doi.org/10.1504/PCFD.2012.047457. http://www.inderscience.com/link.php?id=47457.

Köhler, A., Pallarès, D., Johnsson, F., 2017. Magnetic tracking of a fuel particle in a fluid-dynamically down-scaled fluidised bed. Fuel Process. Technol. 162, 147–156. https://doi.org/10.1016/j.fuproc.2017.03.018.

Li, Z., Kuang, S., Liu, S., Gan, J., Yu, A., Li, Y., Mao, X., 2019. Numerical investigation of burden distribution in ironmaking blast furnace. Powder Technol. 353, 385–397. https://doi.org/10.1016/j.powtec.2019.05.047.

Lichtenegger, T., Peters, E.A.J.F., Kuipers, J.A.M., Pirker, S., 2017. A recurrence CFD study of heat transfer in a fluidized bed. Chem. Eng. Sci. 172, 310–322. https://doi.org/10.1016/j.ces.2017.06.022.

Liu, Z.J., Zhang, J.L., Zuo, H.B., Yang, T.J., 2012. Recent progress on long service life design of Chinese Blast furnace hearth. ISIJ Int. 52, 1713–1723. https://doi.org/10.2355/isijinternational.52.1713.

Mema, I., Buist, K.A., Kuipers, J.A., Padding, J.T., 2020. Fluidization of spherical versus elongated particles: Experimental investigation using magnetic particle tracking. AIChE J. 66, 1–13. https://doi.org/10.1002/aic.16895.

Milacic, E., Baltussen, M.W., Kuipers, J.A.M., 2019. Direct numerical simulation study of droplet spreading on spherical particles. Powder Technol. 354, 11–18. https://doi.org/10.1016/j.powtec.2019.05.064.

Natsui, S., Ueda, S., Fan, Z., Andersson, N., 2010. Characteristics of Solid Flow and Stress Distribution Including Asymmetric Phenomena in Blast Furnace Analyzed by Discrete Element Method. ISIJ Int. 50, 207–214. https://doi.org/10.2355/isijinternational.50.207.

Neuwirth, J., Antonyuk, S., Heinrich, S., Jacob, M., 2013. CFD-DEM study and direct measurement of the granular flow in a rotor granulator. Chem. Eng. Sci. 86, 151–163. https://doi.org/10.1016/j.ces.2012.07.005.

Nijssen, T.M., Kuipers, H.A., van der Stel, J., Adema, A.T., Buist, K.A., 2020. Complete liquid-solid momentum coupling for unresolved CFD-DEM simulations. Int. J. Multiph. Flow 132, 103425. https://doi.org/10.1016/j.ijmultiphaseflow.2020.103425.

Nogami, H., Toda, K., Pintowantoro, S., Yagi, J.I., 2004. Cold-model experiments on deadman renewal rate due to sink-float motion of hearth coke bed. ISIJ Int. 44, 2127–2133. https://doi.org/10.2355/isijinternational.44.2127.

Nouchi, T., Sato, T., Sato, M., Takeda, K., Ariyama, T., 2005. Stress Field and Solid Flow Analysis of Coke Packed Bed in Blast Furnace Based on DEM. ISIJ Int. 45, 1426–1431. https://doi.org/10.2355/isijinternational.45.1426. http://joi.jlc.jst.go.jp/JST.JSTAGE/isijinternational/45.1426?from=CrossRef.

Nouchi, T., Takeda, K., Yu, a.B., 2003. Solid Flow Caused by Buoyancy Force of Heavy Liquid. ISIJ Int. 43, 187–191. https://doi.org/10.2355/isijinternational.43.187. http://joi.jlc.jst.go.jp/JST.Journalarchive/isijinternational1989/43.187?from=CrossRef.

Nouchi, T., Yasui, M., Takeda, K., 2003. Effects of Particle Free Space on Hearth Drainage Efficiency. ISIJ Int. 43, 175–180. https://doi.org/10.2355/isijinternational.43.175. http://joi.jlc.jst.go.jp/JST.Journalarchive/isijinternational1989/43.175?from=CrossRef.

Nouchi, T., Yu, A.B., Takeda, K., 2003. Experimental and numerical investigation of the effect of buoyancy force on solid flow. Powder Technol. 134, 98–107. https://doi.org/10.1016/S0032-5910(03)00121-9.

Omori, Y., 1987. Blast Furnace Phenomena and Modelling. Springer, Netherlands, Dordrecht. https://doi.org/10.1007/978-94-009-3431-3. URL http://link.springer.com/10.1007/978-94-009-3431-3 http://www.springer.com/us/book/9781851660575%5Cnhttp://link.springer.com/10.1007/978-94-009-3431-3.

Panjkovic, V., Truelove, J.S., Zulli, P., 2002. Numerical modelling of iron flow and heat transfer in blast furnace hearth. Ironmaking Steelmaking 29, 390–400. https://doi.org/10.1179/030192302225005187.

Peacy, J., Davenport, W., 1979. The Iron Blast Furnace: Theory and Practice. Pergamon Press, London.

Prosperetti, A., 2002. Navier-Stokes numerical algorithms for free-surface flow computations: An overview. Drop-Surface Interact., 237–257 https://doi.org/10.1007/978-3-7091-2594-6_8.

Richert, H., Kosch, O., Gornert, P., 2006. Magnetic Monitoring as a Diagnostic Method for Investigating Motility in the Human Digestive System. In: Magnetism in Medicine. Wiley.

Rusche, H., 2002. Computational fluid dynamics of dispersed two-phase flows at high phase fractions (Ph.D. thesis). Imperial College of Science, Technology & Medicine (London). URL http://ethos.bl.uk/OrderDetails.do?uin=uk.bl.ethos.402087.

Shao, L., 2013. Model-based estimation of liquid flows in the blast furnace hearth and taphole (Ph.D. thesis). Abo Akademi University.

Shao, L., Saxén, H., 2013. Flow patterns of iron and slag in the blast furnace taphole. ISIJ Int. 53, 1756–1762. https://doi.org/10.2355/isijinternational.53.1756.

Shibata, K., Kimura, Y., Shimizu, M., Inaba, S.i., 1990. Dynamics of dead-man coke and hot metal flow in a blast furnace hearth. ISIJ Int. 30, 208–215. https://doi.org/10.2355/isijinternational.30.208. http://joi.jlc.jst.go.jp/JST.Journalarchive/isijinternational1989/30.208?from=CrossRef.

Takahashi, H., Kawai, H., 2001. Deadman Renewal Motion in a Cold Model of Blast Furnace. Tetsu-to-Hagane 87, 373–379.

Takahashi, H., Komatsu, N., 1993. Cold Model Study on Burden Behaviour in the Lower Part of Blast Furnace. ISIJ Int. 33, 655–663. https://doi.org/10.2355/isijinternational.33.655.

Takahashi, H., Tanno, M., Katayama, J., 1996. Burden descending behaviour with renewal of deadman in a two dimensional cold model of blast furnace. ISIJ Int. 36, 1354–1359. https://doi.org/10.2355/isijinternational.36.1354.

Takatani, K., Inada, T., Takata, K., 2001. Mathematical model for transient erosion process of blast furnace hearth. ISIJ Int. 41, 1139–1145. URL file://hermes26/SCC/CFD/Literature CFD/Blast Furnace/isij411139 Takatani et al. 2001 Mathematical model for transient erosion process of blast furnace hearth.pdf.

Tanzil, W.B.U., Zulli, P., Burgess, J.M., Pinczewski, W.V., 1984. Experimental model study of the physical mechanisms governing blast furnace hearth drainage. Trans. ISIJ 24, 197–205.

Ueda, S., Natsui, S., Fan, Z., Nogami, H., Soda, R., Kano, J., 2010. Influences of Physical Properties of Particle in Discrete Element Method on Descending Phenomena and Stress Distribution in. ISIJ Int. 50, 981–986. https://doi.org/10.2355/isijinternational.50.981.

Vångö, M., Feilmayr, C., Pirker, S., Lichtenegger, T., 2019. Data-assisted CFD modeling of transient blast furnace tapping with a dynamic deadman. Appl. Math. Model. 73, 210–227. https://doi.org/10.1016/j.apm.2019.04.024.

Vångö, M., Pirker, S., Lichtenegger, T., 2018. Unresolved CFD-DEM modeling of multiphase flow in densely packed particle beds. Appl. Math. Model. 56, 501–516. https://doi.org/10.1016/j.apm.2017.12.008.

Volk, A., Ghia, U., Stoltz, C., 2017. Effect of grid type and refinement method on CFD-DEM solution trend with grid size. Powder Technol. 311, 137–146. https://doi.org/10.1016/j.powtec.2017.01.088.

Wu, H., Du, P., Kokate, R., Wang, J.X., 2021. A semi-analytical solution and AI-based reconstruction algorithms for magnetic particle tracking. PLoS ONE 16, 1–18. https://doi.org/10.1371/journal.pone.0254051.

Yagi, J.i., 1993. Mathematical Modeling of the Flow of Four Fluids in a Packed Bed. ISIJ Int. 33, 619–639. https://doi.org/10.2355/isijinternational.33.619. http://www.jstage.jst.go.jp/article/isijinternational1989/33/6/33_6_619/_article.

Yang, F.L., Hunt, M.L., 2008. A mixed contact model for an immersed collision between two solid surfaces. Philos. Trans. Roy. Soc. A: Math. Phys. Eng. Sci. 366, 2205–2218. https://doi.org/10.1098/rsta.2008.0014. http://www.ncbi.nlm.nih.gov/pubmed/18348970.

Yang, L., Padding, J.T., Buist, K.A., Kuipers, J.A.M., 2017. Three-dimensional fluidized beds with rough spheres: Validation of a Two Fluid Model by Magnetic Particle Tracking and discrete particle simulations. Chem. Eng. Sci. 174, 238–258. https://doi.org/10.1016/j.ces.2017.09.014.

Zhang, J.L., Chen, Y.X., Fan, Z.Y., Hu, Z.W., Yang, T.J., Ariyama, T., 2011. Influence of profile of blast furnace on motion and stress of burden by 3D-DEM. J. Iron. Steel Res. Int. 18, 1–6. https://doi.org/10.1016/S1006-706X(11)60108-8.

Zhou, Z., Zhu, H., Yu, A., Wright, B., Pinson, D., Zulli, P., 2005. Discrete Particle Simulation of Solid Flow in a Model Blast Furnace. ISIJ Int. 45, 1828–1837. https://doi.org/10.2355/isijinternational.45.1828.

Zhou, Z., Zhu, H., Yu, A., Zulli, P., 2010. Numerical Investigation of the Transient Multiphase Flow in an Ironmaking Blast Furnace 50, 515–523.